Employing UAS to Perform Low Altitude Navaids Measurements

20th International Flight Inspection Symposium (IFIS) 2018, April 16-20, Monterey, California

Jochen Bredemeyer, *FCS Flight Calibration Services GmbH, Germany*
Thorsten Schrader, *Physikalisch-Technische Bundesanstalt (PTB), Germany*

BIOGRAPHIES

Dr. Bredemeyer received his diploma degree (Dipl.-Ing.) in 1996 and his PhD (Dr.-Ing.) in 2001, both in electrical engineering, from Technische Universität Braunschweig. His present position at FCS is Head of Research. The focus of his work is on RF measurement engineering, signal processing and multipath wave propagation. He is also Honorary Professor at Leibniz Universität Hannover, Faculty of Electrical Engineering and Computer Science, where he lectures on radio navigation and radar.

Dr. Schrader received the Dipl.-Ing. and Dr.-Ing. degrees in electrical engineering from Technische Universität Braunschweig, in 1992 and 1997, respectively. In 1999, Thorsten Schrader joined the Physikalisch-Technische Bundesanstalt (PTB) in Braunschweig. Since 2005 he is the head of the department “High Frequency and Electromagnetic Fields”. His current interest is the metrology of RF quantities up to the millimeter wave and terahertz range including vector network analysis, antennas, dosimetry, electromagnetic compatibility, and UAS-based measurements.

ABSTRACT

An unmanned aerial system (UAS)-based measurement system to supplement or replace ground inspection of ILS (LOC, GP) and (D)VOR is described. This platform allows quasi-stationary hovering not only in areas normally accessed with mast-equipped vehicles for ILS ground inspections, but also in critical areas accessible only with a flying platform. The calibrated and operationally robust UAS is an ideal tool for setting up system and antennas of new installations, thus accelerating the commissioning of ILS Localizers and Glideslopes prior to certification by flight inspection. Measurements are now also possible in locations where it is not practical or safe to measure with a conventional flight inspection system, e.g. to generate measurement data for electromagnetic simulations.

A conventional multicopter is used as a carrier UAS. Dedicated antennas were designed to respond to both electromagnetic and mechanical requirements for the respective wavelengths of 3m (LOC, VOR) and 1m (GP). The UAS features a light-weight dedicated dual ILS LOC/GP (VOR, GBAS) receiver and recorder payload based on a miniaturized, FPGA-controlled system handling large bandwidth data streams in real-time. All components, i.e. antennas, RF and signal processing hard- and firmware were specially designed to meet the application’s requirements.

A particular challenge is to separate the desired ILS/VOR signal-in-space from near field effects generated by the UAS itself. Effects that must be carefully removed from the incoming ADC-sampled signal is e.g. propeller induced amplitude modulation, or the short-term dynamics of a flying UAS.

In contrast to conventional ILS receiver technology, the raw channel bandpass signal-in-space covering the complete channel bandwidth is sampled and directly recorded at a high data rate. Signal postprocessing then extracts all essential parameters of interest. Responding to a main user requirement, essential ILS /VOR parameters are down-linked in real-time. This was implemented through combined hardware and software signal processing. A radio link is connected to a tablet PC on the ground for sensor control and the display of relevant signal parameters.

The paper describes the experience gained with the system, and provides recent measurement results obtained from ILS Localizer/Glidepath and VOR installations.

INTRODUCTION

The multicopter drone (UAS) developed within the frame of the German WERAN[1] project serves as a general carrier for various RF instrumentation equipment. The WERAN focus, i.e. to examine the effects of wind turbines on NAV and radar signal propagation, almost naturally led to the extension of the measurement application towards more "classical" ILS and VOR measurements. This drone is able to complement flight inspection in some areas to detect signal anomalies, and on the other hand it can perform certain ground-based measurements much more effectively than portable receivers connected to antennas on telescopic masts. The drone can very effectively replace the gap between conventional ground measurements and areas or points in airspace that the flight check aircraft cannot reach.

While these near-ground measurements cannot replace flight inspection at larger distances or higher altitudes, an extension of their scope of operation is of course conceivable. However, due to the substantially higher complexity, cost, and the regulative overhead of operating large and complex UAS in an airport environment it remains to be seen if a business case will ever come about.

This paper therefore focusses on the new measurement capabilities for the signal-in-space of conventional Navaids and some fundamental prerequisites for signal analysis on UAS platforms in a near-ground environment. FCS and PTB now have practical experience using such UAS since 2014. The application shown here is the evaluation of ILS antenna patterns and the DDM flight guidance parameter. During deployment phase of new ILS (LOC/PG), UAS measurements are highly useful to accurately adjust the antennas before the start of the commissioning flight check. A mid-term goal is to replace the ILS localizer runway checks with masts-equipped vehicles by a programmed drone with a sensor.

EQUIPMENT

At first glance, assembling UAS (drone) COTS components, a small ILS receiver and an antenna to obtain a measurement system appears simple. But this soon changes when the practical results significantly differ from what is expected, and the reason is not traceable. This paper presents a different approach. The entire system consisting of the UAS as the carrier and all other components, including the payload of a dedicated set of receivers and antennas is regarded as the measurement device.

For testing purposes and comparison, two different UAS platforms with eight brushless motors each were used as carriers (~1 m diameter in the rotor plane) and equipped with dedicated antennas and receivers for ILS LOC/GP and VOR. In Figure 1 a) an octocopter is shown. With this UAS, most of the WERAN measurements for VOR were carried out. Subfigure b) demonstrates an X8-type UAS as the brand's evolving design. Both pictures reveal bow-tie antennas to be used for VHF signal reception.

Since the entire device is the antenna rather than just the radiating elements, a three-dimensional full wave electromagnetic simulation was performed using a detailed CAD model of the UAS. A finite element method (FEM) frequency domain solver was used for this task. This simulation of the "antenna installed performance" shows the effective far field radiation and is the necessary step before building the actual radiator. In case of the octocopter, Figure 2 shows the spherical pattern of the VHF bow-tie antenna. Only after obtaining satisfactory simulation results it is worth building the antenna mechanically to prepare validation efforts. The device was optimized to reduce sensitivity for polarization losses and its construction underwent an iterative optimization. Various test in anechoic chambers and under free-field conditions finally confirmed acceptance. For the ILS GP a short Yagi antenna is used. Its construction underwent the same process as for the bow-tie antenna.

In principle, the receiver concept was described in [3]. Specialized VHF/UHF RF frontends for usage on drones were developed to feed a three-channel intermediate frequency (IF) raw bandpass signal recording system. The full ILS/VOR/GBAS channels are continuously sampled at high bandwidth (>2MHz) using 16Bit A/D converters. Their data streams are recorded on a small 1 TB SSD. Demodulation in real-time and representation of the measurands of interest are computed by a FPGA and an embedded processor. An Android app used by an operator on the ground is connected to the UAS via a separate radio link. This permits full access to all parameters of the RF sensor.

---

[1] In the WERAN project (German abbreviation for "Measuring the potential interaction of wind turbines with terrestrial navigation and radar systems" – supported by the Federal Ministry of Economic Affairs and Energy on the basis of a decision by the German Bundestag [grant: 0325644A]), the potential interaction between wind turbines and terrestrial navigation / radar systems is investigated.

For all applications covered by this measurement drone (ILS, VOR, GBAS), it is always the primary task to analyze the channels' in-band components with respect to the real signals when airborne, before determining any hard-wired demodulation scheme. A deep analysis of signal components is only possible if full bandpass-signal-in-space data is available. Any further processing in time and frequency domain is then possible afterwards. The availability of the recorded bandpass signal is therefore a pre-requisite to develop a well-adapted processing based on bandpass/baseband signal theory described in literature, e.g. [2] .

Regarding GNSS navigation of the UAS, a Novatel OEM615 with INS, magnetic compass, baro altitude and optional RTK is used. Other manufacturers also offer competitive devices with similar claimed accuracy of 10cm vertically.

The overall system is calibrated with reference signals in free space. This allows for absolute field strength measurements traceable to national standards and derivation of an uncertainty [5]. However, the focus of this paper is not to describe this process in detail. As mentioned before, the entire platform represents the measurement system. Therefore, in contrast to normal lab test equipment, there is no need to provide a large table of specific RF parameters. For example, as RF input ports are not accessible, the specification of RF receiver sensitivity level is irrelevant.

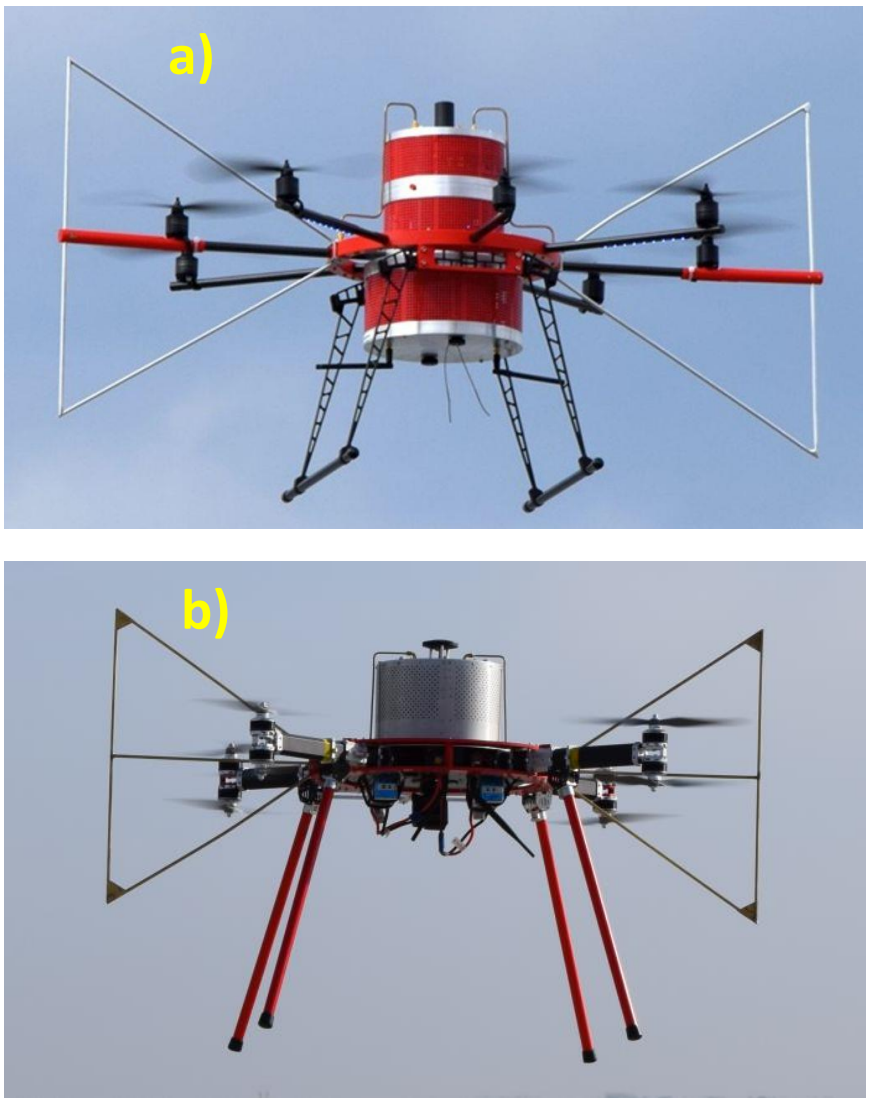

Figure 1: UAS for Navaid inspection; a) Type "Octocopter" b) Type "X8"

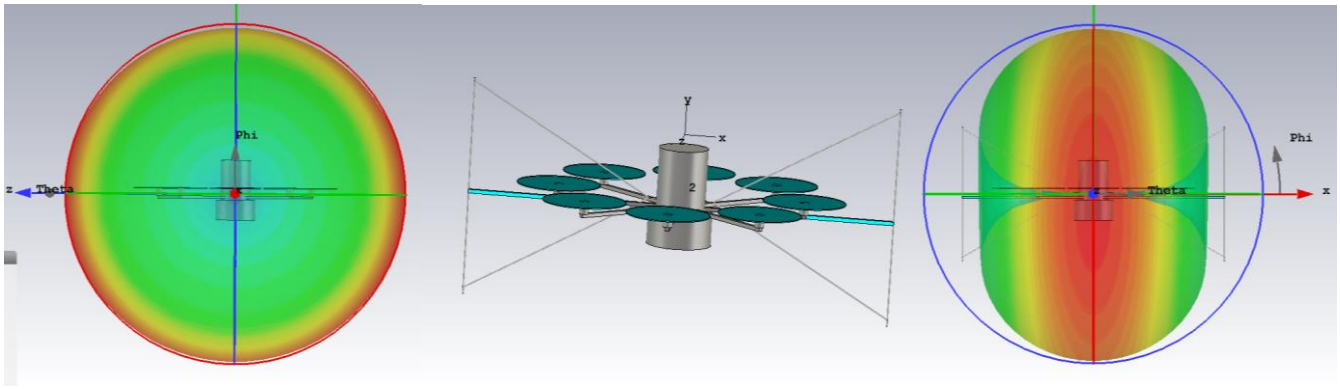

Figure 2: 3D far field patterns of octocopter VHF bow-tie antenna

A CHALLENGE: PROPELLER MODULATION

It is indeed important that a clear distinction is made between the ILS' true signal-in-space and components that might unintentionally be added by the measurement system itself due to its high dynamics.
On a flight inspection aircraft, a turboprop engine's typical rotational speed may be 1500 rpm or above, four blades therefore cause a 4*1500/60s = 100 Hz amplitude modulation (AM) dual sideband spectrum relative to the carrier. During landing, the speed is reduced and so is the AM sideband frequency. This AM can be observed e.g. in the Localizer spectrum. In Figure 3 there is a sequence of the lower sideband (LSB) shown in the vicinity of 100 Hz. The prop AM appears as a crawling spectral line that passes through the ILS 90 Hz tone. Generally, this problem is well known and also described in DOC 8071 [1]{sec. 3.7}. When measuring the DDM, this prop AM caused a large deflection that exceeded +/-20 µA in the depicted scenario.

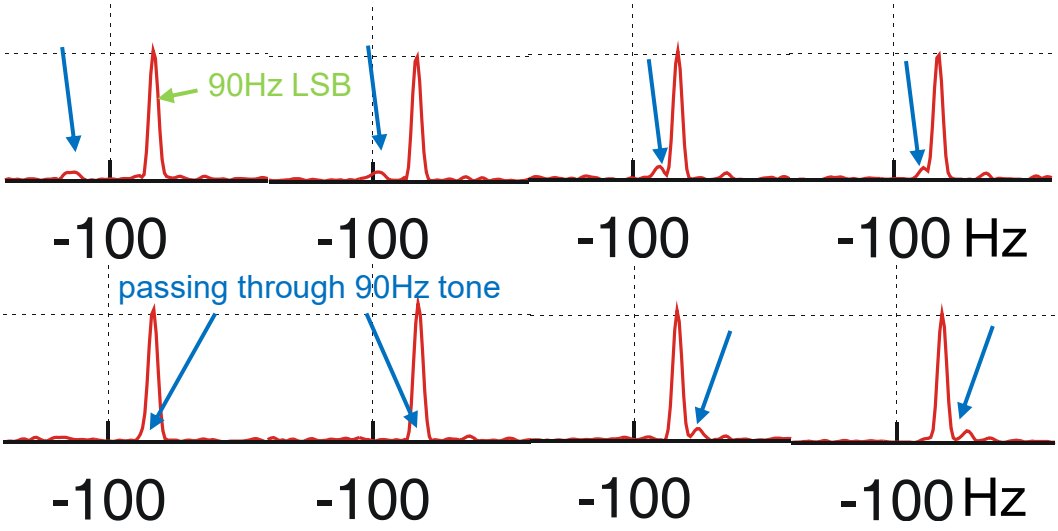

Figure 3: Propeller Amplitude Modulation in LOC spectrum of flight inspection aircraft during landing

On a typical flight inspection aircraft, there is usually a distance of several meters between the ILS measurement antenna and the propellers. In most cases, the number of engines is one or two and the difference in rotation speed is limited. All in all, this keeps the number of additional spectral lines small.

Things look markedly different, however, in case of a small UAS with eight motors. To keep the drone stable in the air, a large propeller rpm range will be passed through by each motor. The individual motors are neither synchronized nor adjustable from outside the electronic speed controller, and it is not intended to modify the controller. As shown in the pictures of Figure 1 , the drone propellers are very close to the radiation elements. A complex interaction can be expected.

ILS LOC/GP MEASUREMENTS

LOC Prop AM

As the RF bandpass signal is available as a large set of un-interrupted ADC samples, any operation in the time or frequency domain can be performed. All receiver and navigation data streams are synchronous in time. In context with the preceding section, some examples of prop AM with real ILS signals are given and discussed.

A Short-Time Discrete Fourier Transformation (STDFT) is applied to the ILS localizer signal as shown in Figure 4 when using the octocopter drone. The observation time is one second which allows for sufficient spectral resolution. In a) the UAS is on the runway with the bow-tie antenna very close to the ground some km in front of the LOC antenna. This explains the low signal level. The spectrum is clean when the engines are off, revealing a 60 dB ratio to noise of the useful signal. After the UAS' take-off, the spectrum is substantially cluttered as the spectrum in subfigure b) gives impressive evidence. In contrast to prop AM of a flight inspection aircraft with single lines, a wider part of the spectrum is affected. Since the motors are extremely close to the antenna in terms of wave-lengths, prop AM is very strong This is a physical effect which can be mitigated to some extent by careful selection of the propeller material (wooden propellers being superior to fiberglass ones).

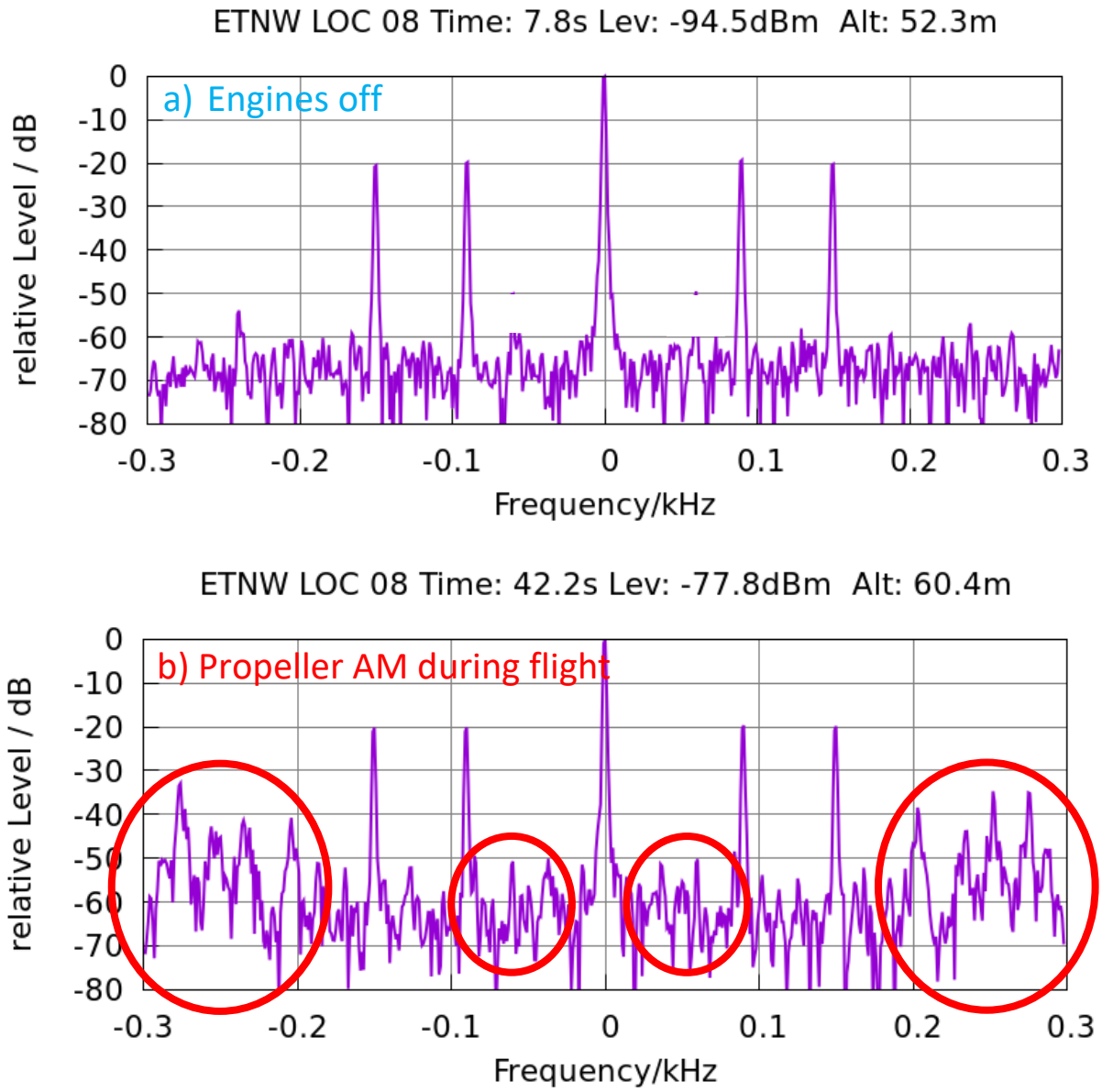

Figure 4: Octocopter: Differences in spectral purity of Localizer bandpass signal; a) clean: engines off; b) cluttered by Prop AM

GP Prop AM: Octocopter

In the following, some glide path results are shown. In the frequency domain, Figure 5 shows some cases of different flight conditions of the octocopter. On ground with motors off a), the GP spectrum is clean as it was in case of the preceding LOC example. The flight profile, named “I profile” consisted of an ascent to an altitude of 100 above ground at a certain point with several hovering steps, then a descent back to ground, 500m in front of a GP mast.
During hovering b) parts of the Prop AM affect the 90Hz ILS tone with very close-by spectral components. Within the following ascent, the engines increase their speed which pushes the interfering lines a few Hertz away from the 90 Hz tone.

The question of course arises to what extent this affects the DDM measurement. A time domain signal processing performed on the bandpass signals and the subsequent baseband provides the results. In Figure 6, an excerpt of the flight showing several parameters against the flight time scale is depicted. In the first half of that period the octocopter was hovering, expressed by the altitude and elevation angle curves. In the top subfigure the DDM reveals an increased roughness which is due to the interfering spectral Prop AM lines within the 90 Hz tone. In the second half, the octocopter ascends and the DDM gets quite smooth. It reaches DDM=0 when passing 3° elevation. The time stamps of the diagrams in Figure 5 correspond to the flight time scale in in Figure 6. As an interim conclusion, the flight maneuver dominates the roughness of DDM due to different spectral distribution of the Prop AM. To obtain a smooth DDM, steep digital filters (FIR type, Finite Impulse Response) with high pole count (a few hundred) must be implemented in baseband signal processing.

In an interative process, the propellers of the octocopter were optimized regarding length, material and number of blades. Not all blade materials were found suitable. Some plastic propellers types with reduced prop AM heavily degraded the octocopter’s flight stability due to their low rigidity. Fiberglass blades offer a better performance.

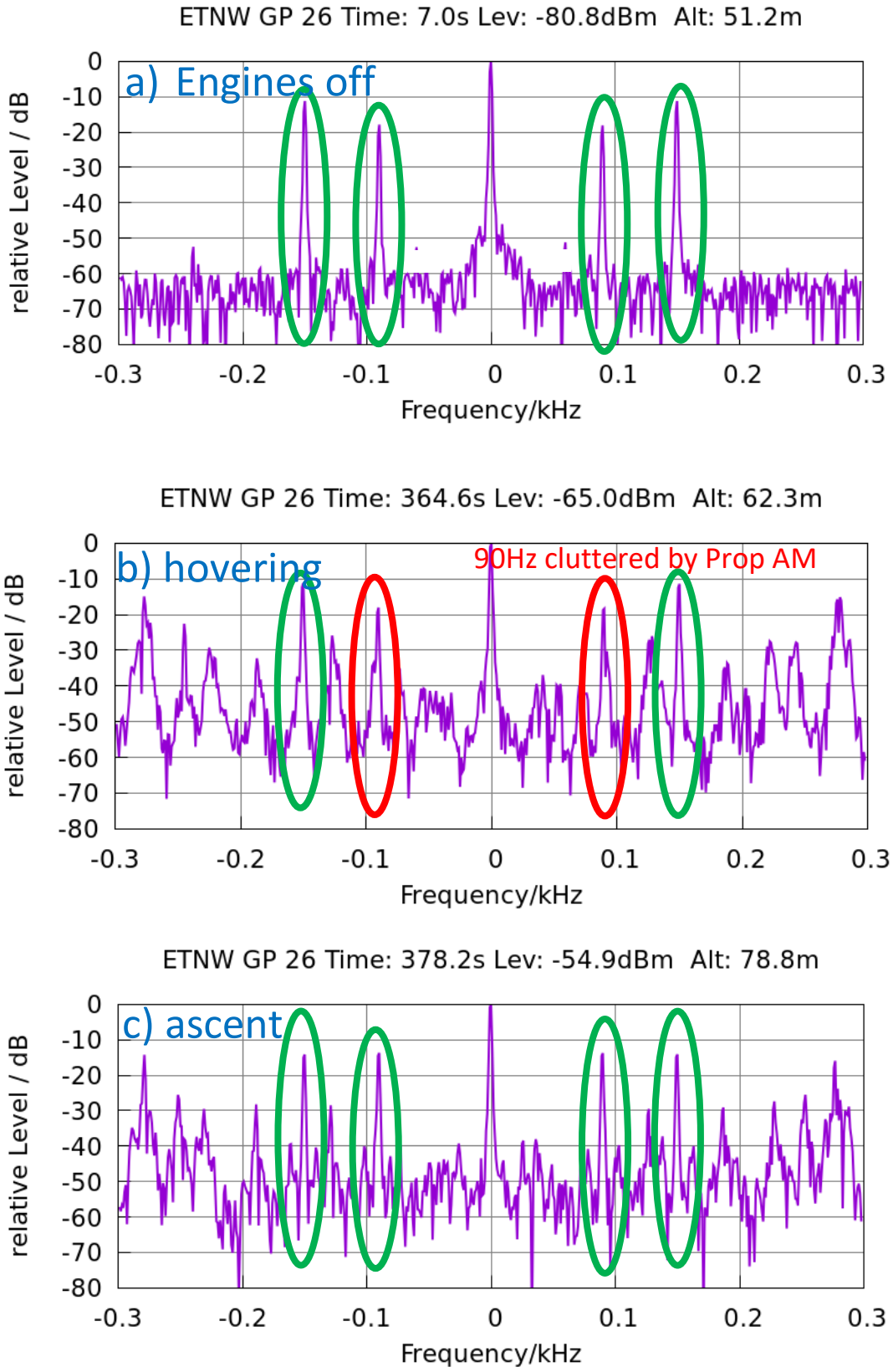

Figure 5: Octocopter: Differences in spectral purity of Glidepath bandpass signal; a) clean: engines off; b) cluttered 90Hz line; c) propeller modulation away from 90/150Hz

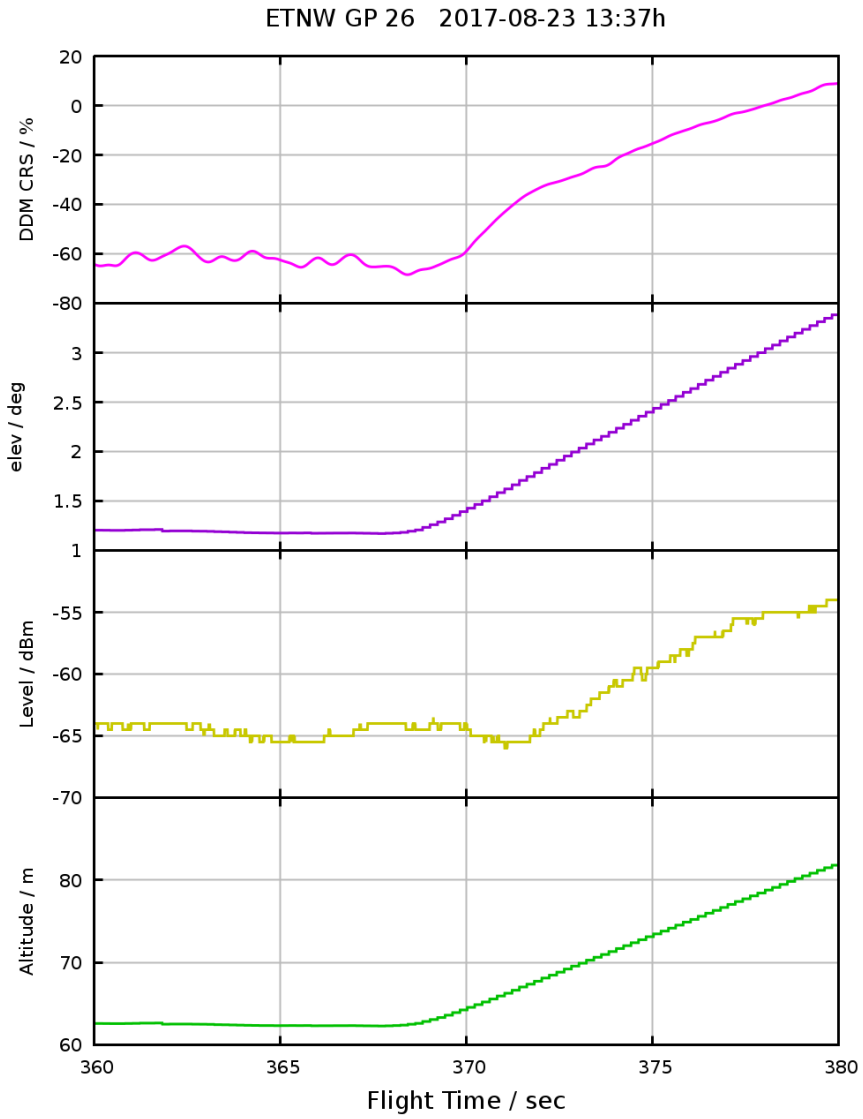

Figure 6: DDM roughness decreases during the octocopter's ascent

GP Prop AM: X8

The X8-type UAS reveals a different behavior. The flight stability of the X8 platform itself allows for other blade materials with a lower relative permittivity.

In Figure 7 the spectrum gained from STDFT of the X8 glidepath measurements are shown. On ground a) with engines switched off a clean spectrum is visible. Flying the "I profile" during ascent b) some more lines appear in the spectrum due to prop AM. However, this spectrum neither broadens to an extent that has been observed with the octocopter in Figure 6 b), nor does it reach a high depth in modulation. Nearly the same applies to the descent c). The additional spectral lines do not harm the useful signal in the closest vicinity of the ILS tones 90/150 Hz.

In the corresponding DDM curve of Figure 8 (top) a smooth course of the curve for both the ascent and the descent can be observed across flight time and altitude/elevation angle.

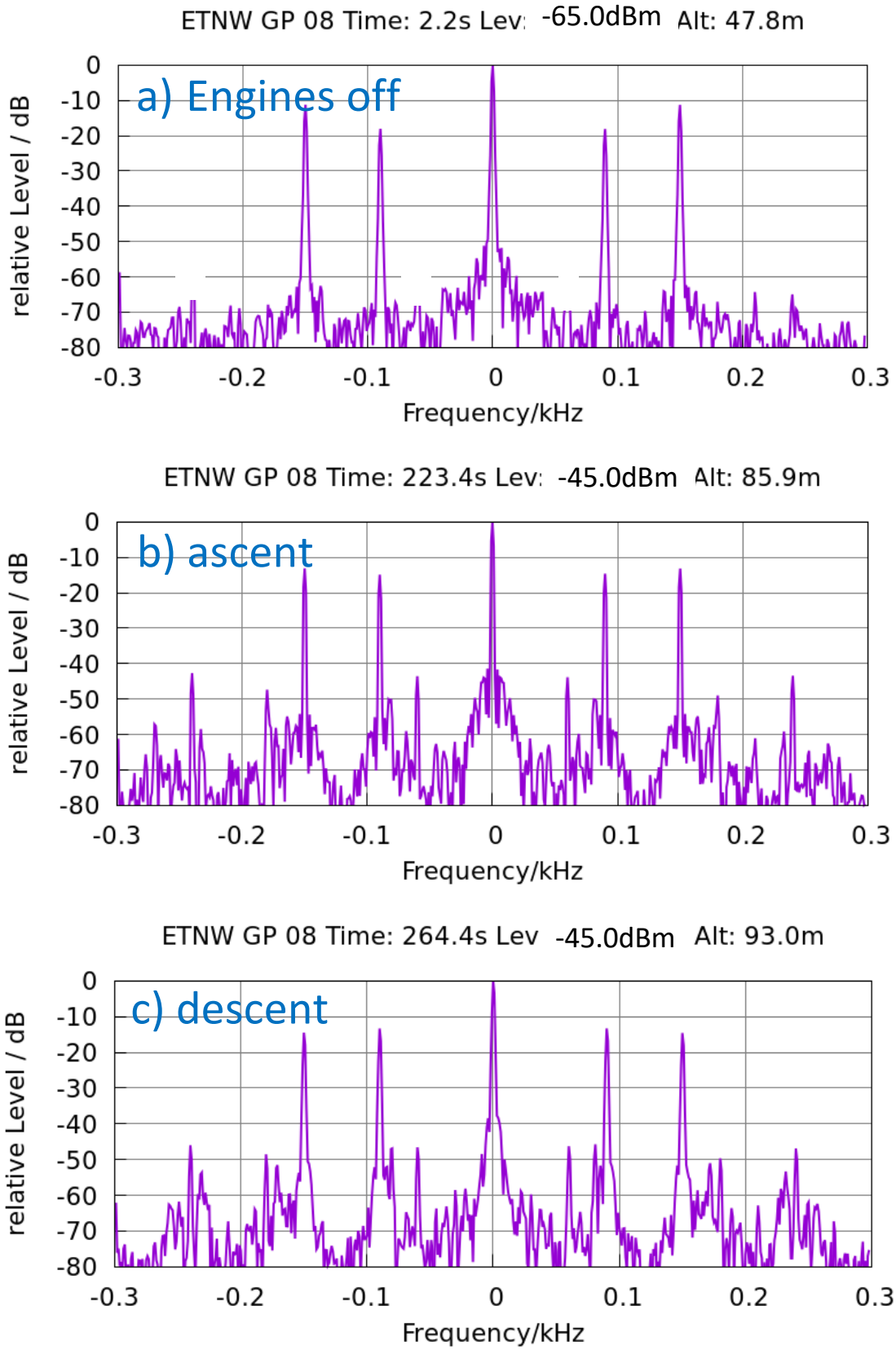

Figure 7: X8: Differences in spectral purity of RF bandpass signal; a) clean: engines off; b) ascent and c) descent: little spectral clutter

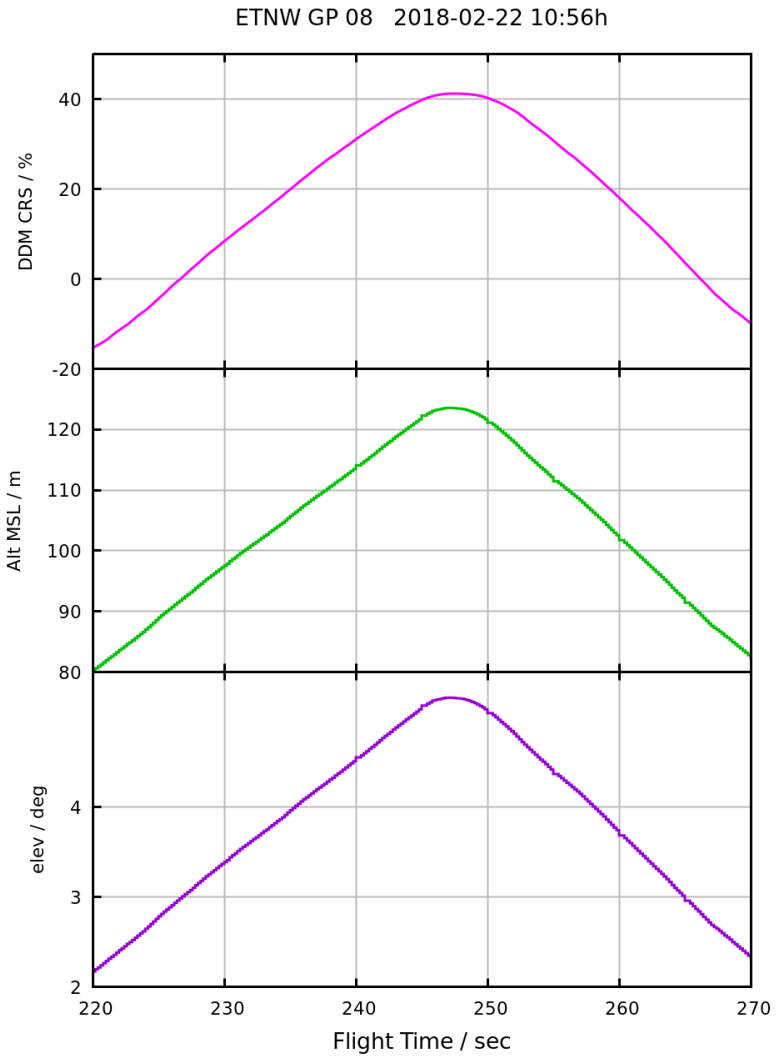

Figure 8: Stable glidepath DDM during ascent and descent of X8

ILS LOC ANTENNA PATTERN MEASUREMENTS

Apart from the DDM as the significant value, it may be of interest to measure the antenna diagrams of CSB (carrier and sidebands) and SBO (sidebands only) separately, for course (CRS)/clearance (CLR) each.

On an airport with a ILS CAT III installation some flight trials were conducted. In Figure 9 two orbit flight paths at distances of 200 m and 1200 m respectively from the LOC antenna are shown on the airport surface.

In case of CSB the CRS/CLR antenna pattern can be measured using the carrier's signal strength. Switching off CSB (or, technically: switching it to a dummy load), the SBO remains. The SBO signal strength cannot be determined in the time domain using conventional AM demodulation due to the missing carrier. In order to derive the SBO signal strength anyway, its frequency spectrum is helpful.

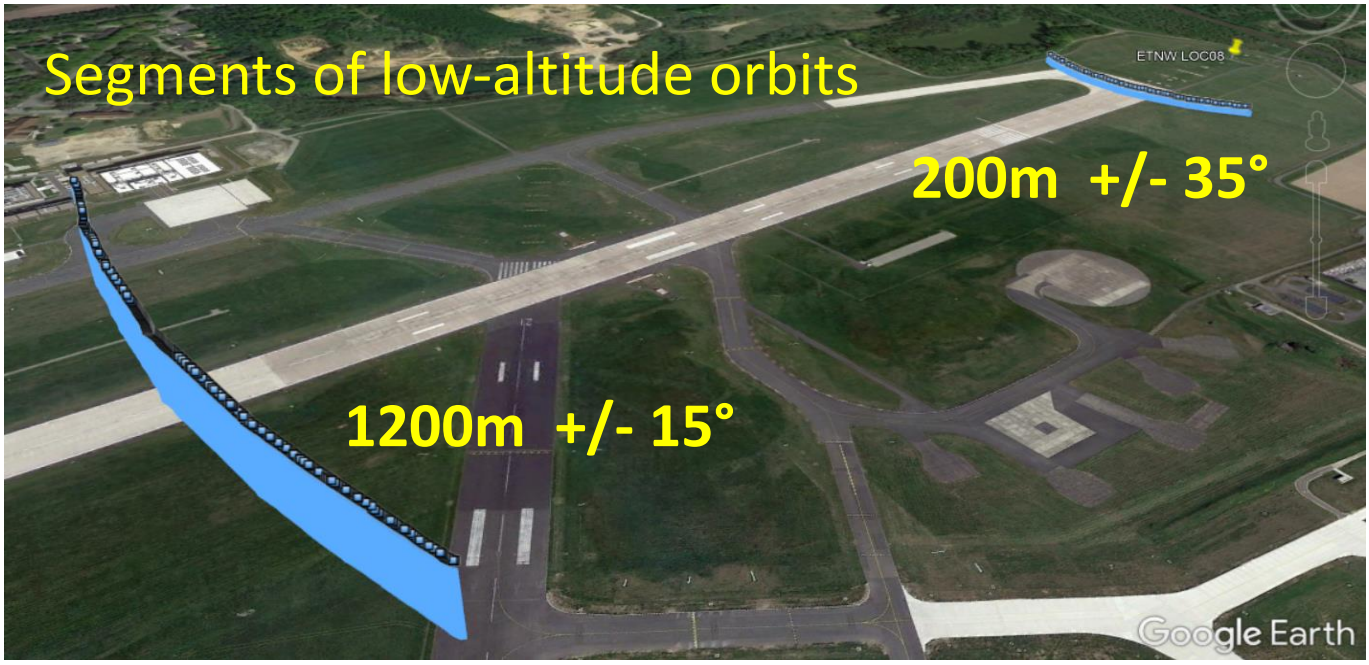

Figure 9: Flight profiles for LOC antenna measurements

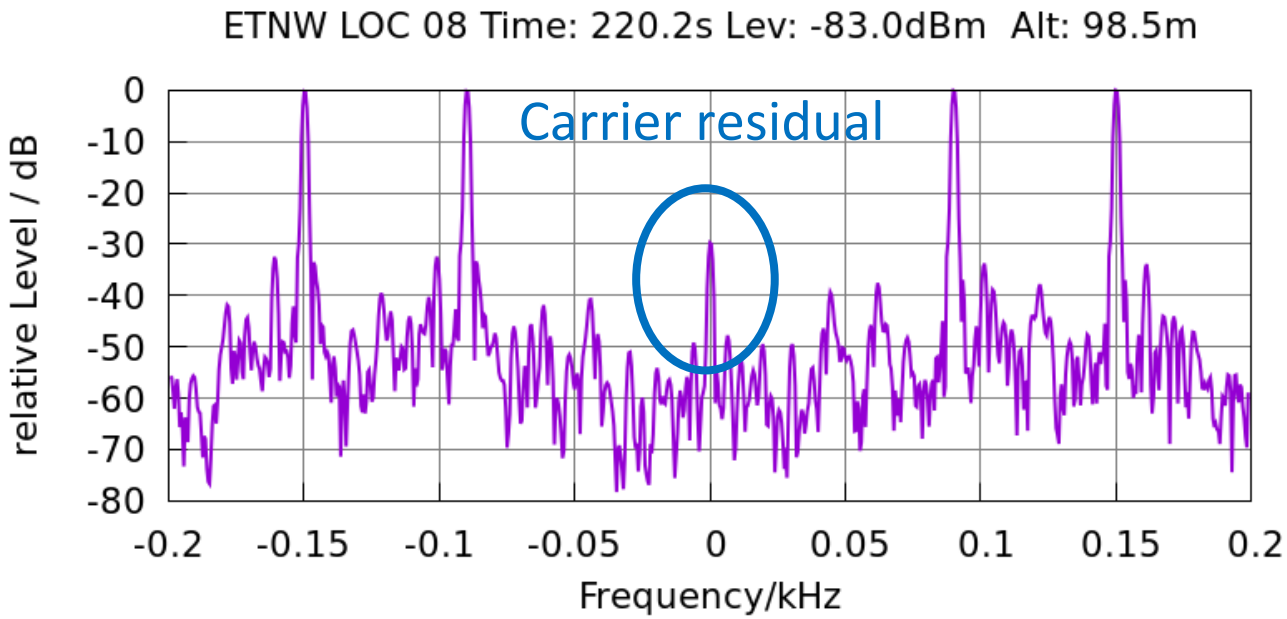

Figure 10: LOC SBO spectrum with residual carrier

In a full ILS spectrum the overlay of CSB and SBO causes the characteristic DDM across the angle deviation which results in different levels of the 90/150 Hz tones (see Figure 4). With SBO alone there is no difference in tone levels, no matter where the signal is probed (the same applies for the tones in case of CSB only). In Figure 10, such a SBO spectrum is shown. It is noticeable that there a carrier is still clearly discernible which is 50 dB below its regular strength when switching on CSB. The reason for the residual carrier is an unavoidable coupling between cables, since the transmitter is still generating CSB at full power fed into the dummy load.

The total SBO signal strength is then gained from the addition of the four spectral tone line magnitudes to obtain a maximum signal-to-noise ratio. Its result varies according to the deviation from centerline, and reflects the horizontal antenna diagram at a certain height and distance.

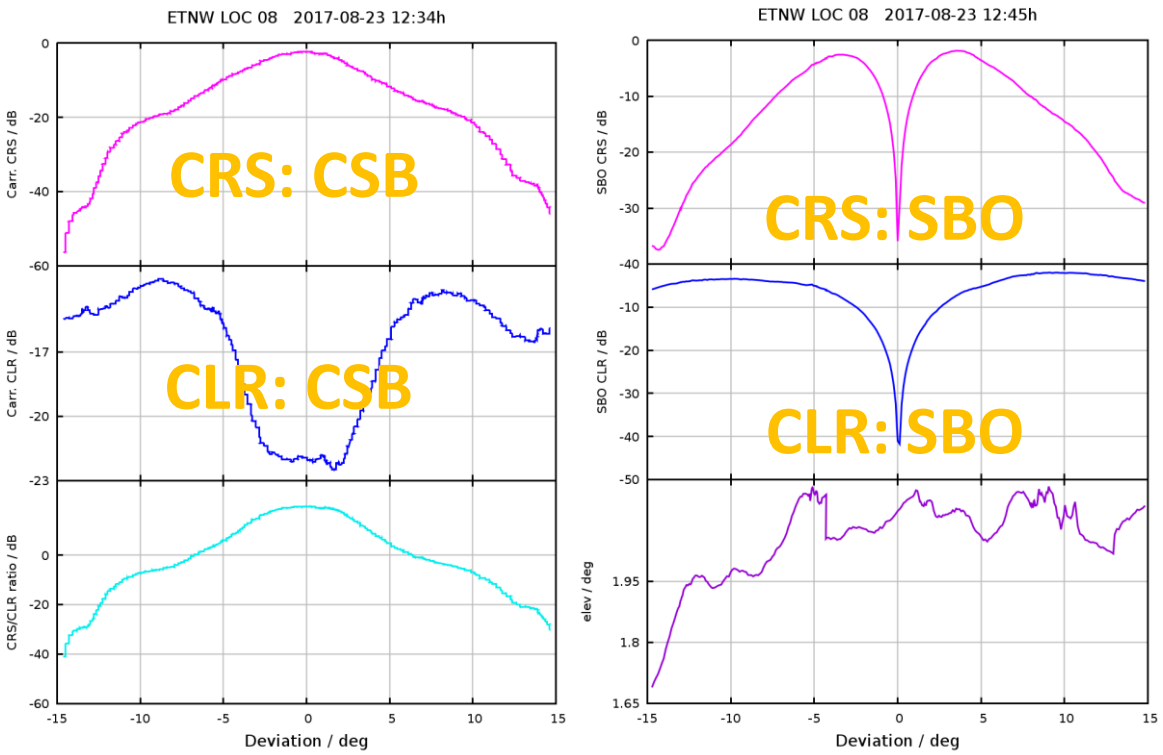

Figure 11: Four measured LOC antenna diagrams at 200 m

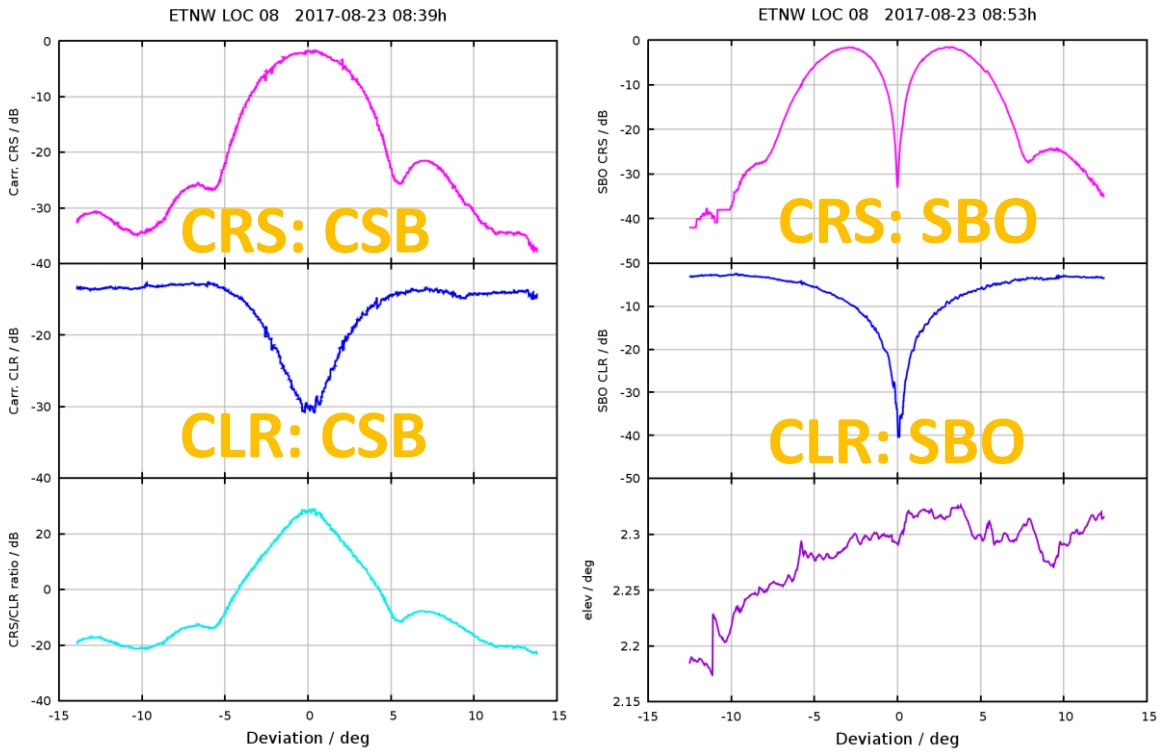

Figure 12: Four measured LOC antenna diagrams at 1200 m

Since the recorded bandpass signal covers the full ILS channel at a high sampling rate it is easy to derive the CRS/CLR ratio directly from the frequency domain in high resolution, just calculating the ratio of their carrier magnitudes.

In Figure 11 and Figure 12 the measured antenna patterns from the orbital flights at two distances are illustrated. On the left, the CSB signal strengths for CRS and CLR plus their ratio is presented, on the right there are the SBO patterns and the elevation angle. The plotted deviation angles are limited to +/-15° to allow for a direct comparison at the two distances.

The closer 200 m distance from the LOC antenna widens the SBO and CSB antenna diagrams. It must be noted that true far field conditions do not exist in a real environment. Since the horizontal antenna aperture is greater than 50 m a distance of 200 m cannot be considered as “far”. From the data sheet of this antenna type (21 el. 2F wide-aperture) a first CSB sidelobe at +/-7° is known. At a distance 1200 m it appears in the measured pattern of Figure 12 (top left), whereas it is unrecognizable at 200 m as shown in Figure 11.

Finally, Figure 13 (left) shows the DDM of CRS, CLR and some parameters more across the deviation from centerline at 1200 m distance. In the right subfigure the X axis represents a small time interval to show some parameters in high resolution when passing through centerline. All curves in that diagram related to the UAS position show a granularity of 5 Hz, which is the data rate of the GNSS device. From the top DDM CRS curve progression it can be read that the deviation resolution is better than 1 µA.

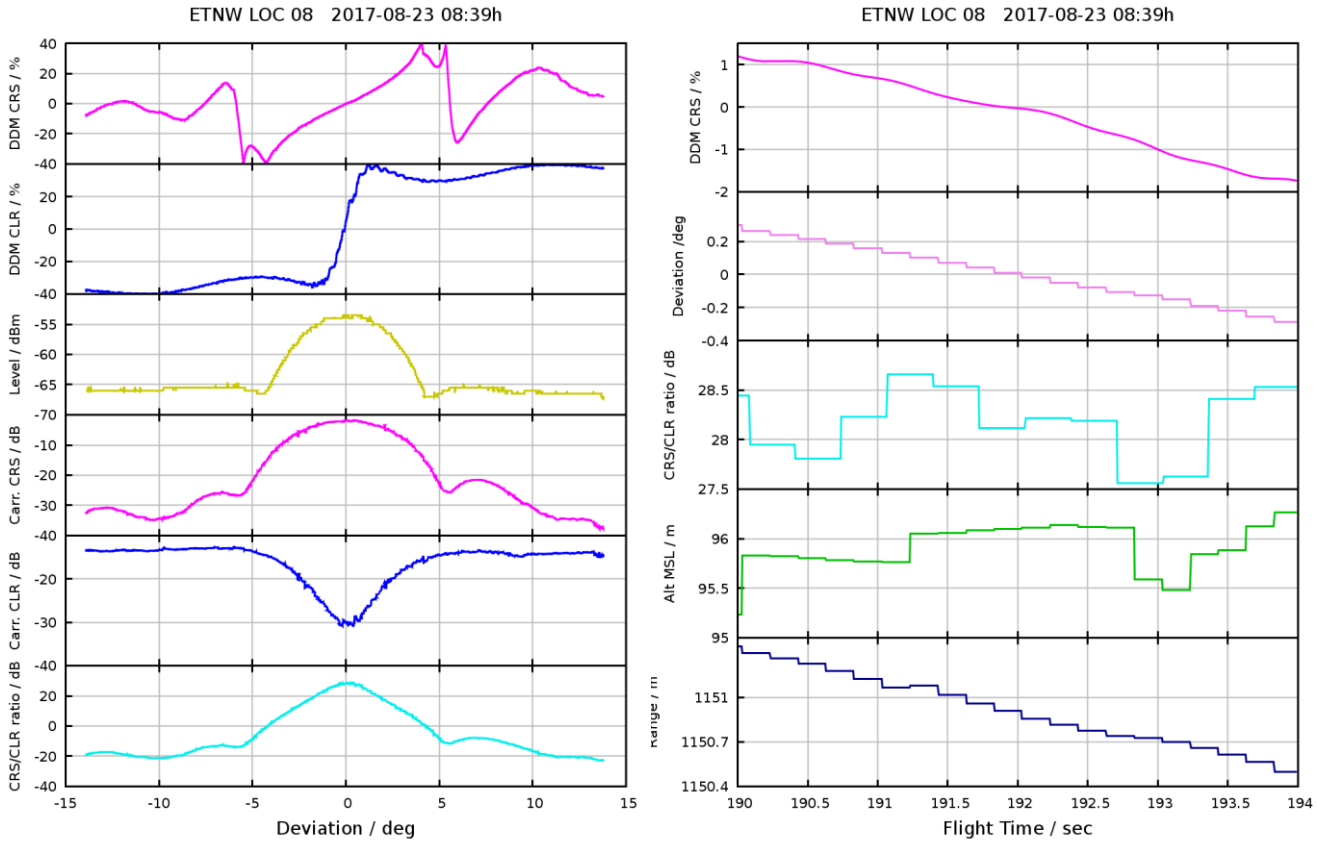

Figure 13: DDM at 1200m across centerline

VOR MEASUREMENTS

A drone might be also useful to check CVOR and DVOR installations near ground during commissioning, before the costly flight inspection takes place. Especially in case of a Doppler VOR, the high complexity of installing the numerous sideband antennas and their respective cables often leads to incorrect connections. Moreover, the fixed monitor antenna in the vicinity of the DVOR and the output of its receiver does not reveal all types of possible erroneous installations.

In the signal processing chain of the UAS presented here, all processing after the of IF signal hardware, A/D sampling and feeding into the FPGA, is done in software. This can be either processed in real-time directly on the FPGA with programmed logic or, for the baseband operations which are less computationally intensive, using the embedded processor and its firmware. Alternatively, the target value of interest can be derived in a postprocess working on the recorded bandpass signal. The latter is used in this example to give profound insights into the DVOR signal. The UAS took off from ground at a specific azimuthal position to the DVOR. A picture by the on-board camera in Figure 14 shows the UAS pointing to the DVOR facility.

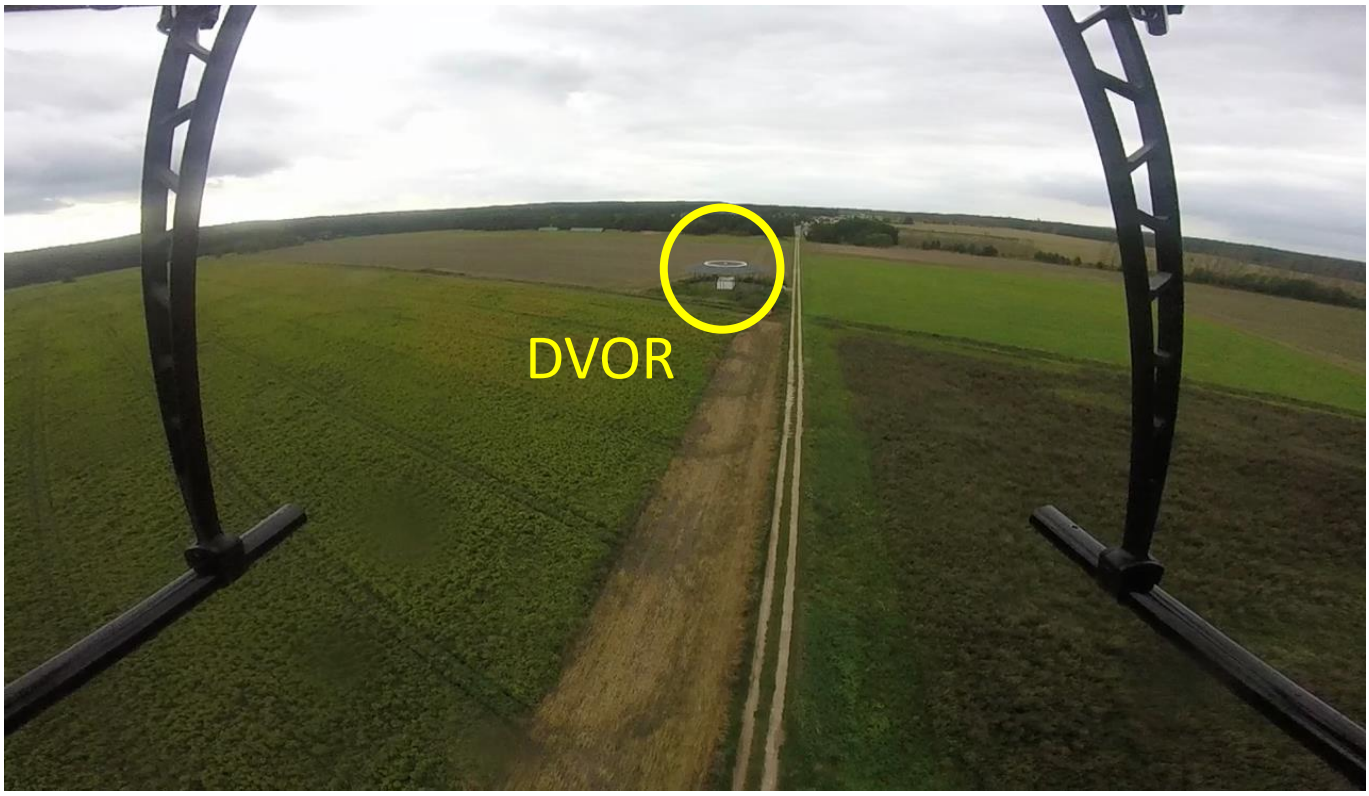

Figure 14: DVOR picture taken from the UAS on-board camera

For a DVOR installation with 50 SBO antennas each of these is active over a period 1/(50*30Hz) = 0.67 ms for both the upper and lower sideband. Since there is no hard-switching of single antennas but a smooth transition, a blending modulation of 750 Hz for upper and lower sideband, sine and cosine half−wave, is introduced. Following the Nyquist criterion, the sample rate must be at least twice the signal's bandwidth, which is roughly 25 kHz for a VOR channel. Assuming a sample rate of 100 kHz, the criterion is fulfilled a will certainly allow to derive the VOR bearing. However, this is unsuitable for the analysis of a single SBO antenna because it would only provide 67 samples each.

It is useful to analyze the SBO antennas in the frequency domain to obtain their signal strength, so the STDFT must be applied. Using a high sampling rate >2 MHz , the observation time is dramatically reduced to less than 1 ms to allow for visualizing the signal strength of the two participating SBO antennas (due to blending modulation) in both sidebands and their respective frequency deviation from their auxiliary AM carriers +/-9.96 kHz. Two short spectral glimpses are given in Figure 15 . Seen from the drone, these two situations represent the maximum Doppler shift of one SBO half cycle in opposite direction. This is

also given by the differences in time (see headlines) which is roughly 1/(2*30Hz) = 0.017s . Reduction in observation time also reduces the spectral resolution. As a consequence, the Doppler shift can only be read with greater uncertainty and will not give the exact opposite deviation, e.g. +480 Hz and -480 Hz. Furthermore, the 30 Hz AM tone is hidden by the carrier. Concatenated pictures of a full SBO cycle, displayed as a movie, are very useful for teaching how the Doppler VOR really works. It is part of the author's university lectures.

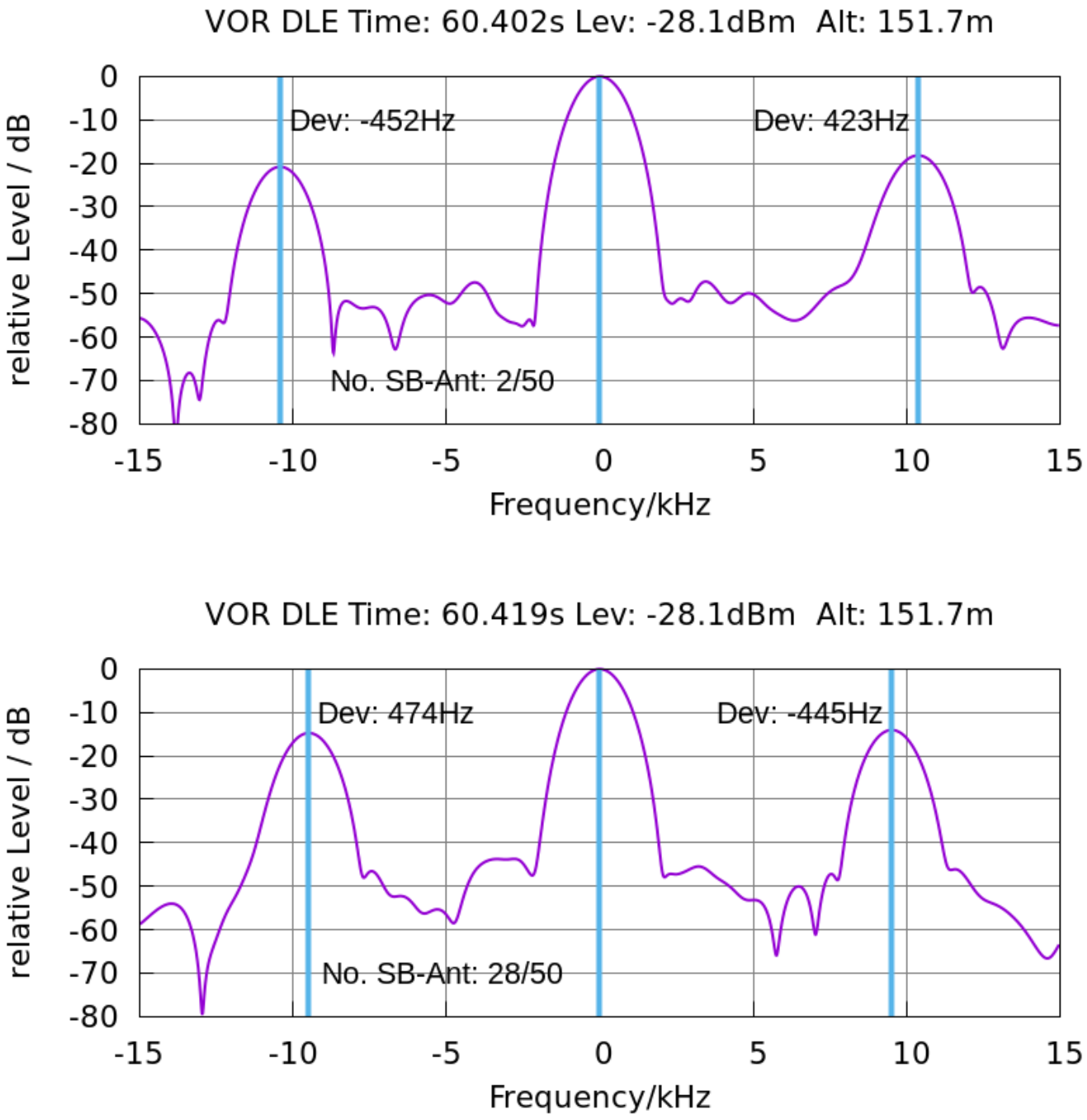

Figure 15: Short-Time DFT to visualize single SB antenna switching with frequency deviation, limited resolution due to short observation time.

If anything goes wrong with the 50 SBO antennas due to wrong cabling, transmitter failure, etc. (which was not the case with this operational DVOR installation) this will appear in the spectral representation. The measured current Doppler shift as depicted in Figure 15 and the correlation between the receiving direction and the SB antenna numbering scheme allows to easily identify the specific faulty antenna.

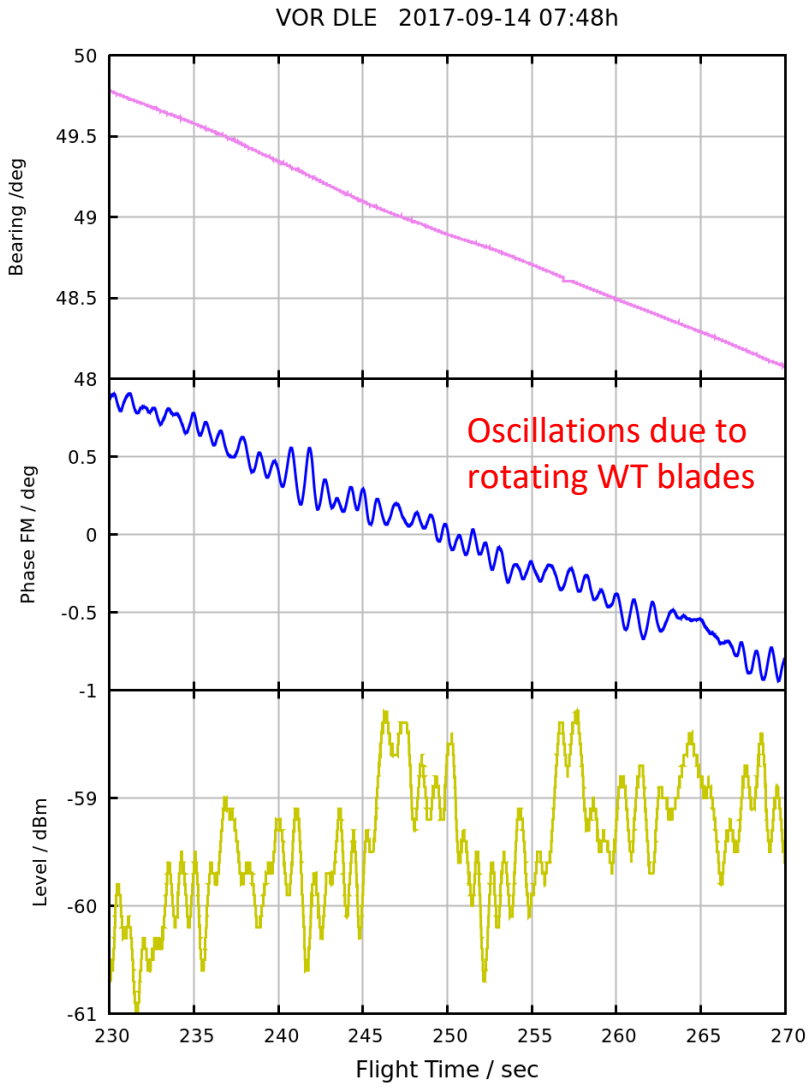

Figure 16: DVOR FM component impaired by wind turbine

A detailed baseband processing of the recorded signal enables the distinction between the AM and the FM 30 Hz tones and their phases. In case of a DVOR, the FM phase represents the bearing information. This FM phase can be derived independently from the signal, and a measurement example of a horizontal flight is given in Figure 16 . The upper curve shows the actual bearing according to the drone's current position. Below, there is the curve progression of the FM phase (without north reference) that shows a significant oscillation. This was due to a line of rotating wind turbines that were passed by during that part of the flight, as shown from the on-board camera in Figure 17 . In the WERAN project, one of the objective was to produce the metrological evidence of angular error that one or more wind turbines (WT) add to the DVOR signal-in-space [4]. It was possible to show that the magnitude of deviation is correlating well with DVOR scattering simulations (not present here, but details given in the named literature).

Figure 17: Flight pattern along wind turbines

CONCLUSIONS

Generally, a UAS with appropriate sensors and signal processing, either in real-time or in post processing, is a very valuable tool to measure detailed signal properties and antenna diagrams of Navaid facilities near ground. Especially in commissioning scenarios or to analyze performance issues, substantial time and cost may be saved to correct the installation, before calling in a flight inspection.

It could be proven that the metrological values of interest, e.g. DDM for ILS and bearing for VOR, can be derived in sufficiently high resolution for this purpose.

According to the multi-year experiences made with various ground systems (Navaids, radar) and situations, a carefully integrated composite UAS system with specially designed elements for Navaid signal-in-space measurements is superior for this task compared to systems assembled from available COTS components and receivers. This specially applies to the availability of a recorded bandpass for in-depth signal processing.

Since the sensor development and software for a large range of Navaids has reached a high degree of maturity, the next development steps will focus on the operation of the UAS in a BVLOS (Beyond Visual Line of Sight) environment. The technology currently under test is U:CON, which will make the UAS position visible to ATC via the LTE mobile network in real-time [6].

REFERENCES

[1] ICAO DOC 8071, Volume I, Testing of Ground-based Radio Navigation Systems, Fourth Edition – 2000

[2] Proakis, J.; Salehi, S: Fundamentals of Communication Systems; Pearson Education, 2nd Edition, 2014

[3] Schrader T.; Bredemeyer J.: Signal-in-space Measurements using Microcopters. 19th International Flight Inspection Symposium (IFIS) 2016, Belgrade, Serbia

[4] Schrader, T.; Bredemeyer, J.; Stupperich, Ch.; Garbe, H.; Mihalachi, M.; Ulm, D.; Sandmann, S.: Interaction of Wind Turbines with VHF Omnidirectional Radio Ranges. Specialist Meeting about Electromagnetic Waves and Wind Turbines, EMWT2017, December 6-7 2017, Braunschweig

[5] JCGM 100:2008. Evaluation of measurement data — Guide to the expression of uncertainty in measurement (GUM)

[6] Heidger, R.: Presentation at CORUS (Concept of Operation for EuRopean UTM Systems) workshop, January 23–24 2018, Barcelona, Spain